

Molecular Physics

An International Journal at the Interface Between Chemistry and Physics

ISSN: 0026-8976 (Print) 1362-3028 (Online) Journal homepage: <https://www.tandfonline.com/loi/tmph20>

Calculation of contact densities and Mössbauer isomer shifts utilising the Dirac-exact two-component normalised elimination of the small component (2c-NESC) method

Terutaka Yoshizawa, Michael Filatov, Dieter Cremer & Wenli Zou

To cite this article: Terutaka Yoshizawa, Michael Filatov, Dieter Cremer & Wenli Zou (2019) Calculation of contact densities and Mössbauer isomer shifts utilising the Dirac-exact two-component normalised elimination of the small component (2c-NESC) method, Molecular Physics, 117:9-12, 1164-1171, DOI: [10.1080/00268976.2018.1530463](https://doi.org/10.1080/00268976.2018.1530463)

To link to this article: <https://doi.org/10.1080/00268976.2018.1530463>



Published online: 05 Oct 2018.



Submit your article to this journal [↗](#)



Article views: 61



View Crossmark data [↗](#)

Calculation of contact densities and Mössbauer isomer shifts utilising the Dirac-exact two-component normalised elimination of the small component (2c-NESC) method

Terutaka Yoshizawa^{a,b}, Michael Filatov^{a,c}, Dieter Cremer^a and Wenli Zou ^{a,d}

^aDepartment of Chemistry, Southern Methodist University, Dallas, Texas, USA; ^bDepartment of Chemistry and Biochemistry, Graduate School of Humanities and Sciences, Ochanomizu University, Bunkyo-ku, Tokyo, Japan; ^cDepartment of Chemistry, Kyungpook National University, Daegu, South Korea; ^dInstitute of Modern Physics, Northwest University, Xi'an, Shaanxi, People's Republic of China

ABSTRACT

Utilizing the analytic derivative formalism for the Mössbauer isomer shift in connection with the Dirac-exact two-component Normalized Elimination of the Small Component (2c-NESC) method a new approach to the analytic calculation of the contact densities at the nuclei has been developed and implemented in the general purpose NESC programme. The new approach is applied to the calculation of the contact densities as well as contact density differences in several iodine-, gold-, and mercury-containing molecules. Substantial differences between the contact densities obtained by the spin-free 1c-NESC method and the 2c-NESC method are found, which demonstrate the importance of spin-orbit coupling. However, the influence of spin-orbit coupling on the contact density differences between the sample and the reference nuclei is found to be modest. This result suggests that a low-cost determination of accurate contact densities at the nuclei can be achieved by combining the 1c-NESC densities obtained at the correlated wavefunction level of theory with the contact density differences obtained at the 2c-NESC/DFT level.

ARTICLE HISTORY

Received 21 July 2018
Accepted 19 September 2018

KEYWORDS

Mössbauer spectroscopy; contact density; normalised elimination of the small component; X2C; spin-orbit coupling






1. Introduction

The contact density is a property which is determined by the electronic wavefunction in the vicinity of the nucleus (also called *the electronic density at a nuclear position*) and is highly sensitive to relativistic effects primarily caused by the mass-velocity and spin-orbit coupling (SOC) terms. Although the absolute value of the contact density is defined by the core electrons closest to the nucleus, its tiny variations due to the changes in the valence electronic shells are amplified through the magnitude of the electron-nucleus contact interactions; thus making it a very sensitive probe of the valence electronic structure. For example, the contact spin-density defines the leading-order relativistic contributions to the nuclear magnetic

shielding constants or the nuclear spin-spin coupling constants through the Fermi contact magnetic interactions [1]. The total (spinless) contact density defines a shift of the energy of the nuclear γ -transition, the so-called isomer shift, in Mössbauer spectroscopy [2]. There are various manifestations of the electrostatic interaction between isotopic nuclei and the contact density, e.g. the 'anomalous mass effect' in chemical reactions of heavy elements [3].

Perhaps the most sensitive method of determining the contact density variations is Mössbauer spectroscopy [2], where the shift of the nuclear γ -transition, measured in the units of velocity needed to reach resonance between the target (A) and the reference (R) nuclei, is assumed to

CONTACT Wenli Zou  zowl@nwu.edu.cn  Department of Chemistry, Southern Methodist University, 3215 Daniel Avenue, Dallas, Texas 75275-0314, USA; Institute of Modern Physics, Northwest University, Xi'an, Shaanxi 710127, People's Republic of China

 Supplemental data for this article can be accessed here. <https://doi.org/10.1080/00268976.2018.1530463>

depend linearly on the respective effective densities ρ_A^{eff} and ρ_R^{eff} , i.e.

$$\Delta_{IS} = \alpha \left(\rho_A^{\text{eff}} - \rho_R^{\text{eff}} \right) \quad (1)$$

where Δ_{IS} is the isomer shift and α is a nuclear calibration constant [4]. The calibration constant is typically determined by a linear regression of the theoretically calculated (effective) contact densities vs. the experimentally measured isomer shifts (cf. Ref. [5,6] and references cited therein). The effective densities ρ_A^{eff} and ρ_R^{eff} are often replaced by contact densities $\bar{\rho}_A$ and $\bar{\rho}_R$, respectively, which in principle may be calculated analytically (see below). It has been found that the replacement may introduce a systematic overestimation to Δ_{IS} (being about 10% for some compounds of Hg [7], Pb [8], and Tl [8]) but can be incorporated into the prefactor α .

As the isomer shift of Mössbauer spectroscopy is a sensitive probe of the chemical environment of the resonating nucleus, the theoretical determination of the contact densities and the (element dependent) calibration constants is of the utmost importance for obtaining detailed information on the electronic structure of inorganic and biological compounds [5,6,9–14]. The elements which can be measured by Mössbauer spectroscopy include iron (^{57}Fe), tin (^{119}Sn), zinc (^{67}Zn), gold (^{197}Au), mercury ($^{199,201}\text{Hg}$), and many rare earth elements such as ^{151}Eu ; altogether more than 40 different transition elements.

As the contact densities are dominated by the deep core electrons (1s shell), relativistic effects need to be taken into account, even for relatively light atoms, such as iron ^{57}Fe [15,16]. It is also essential to incorporate electron correlation effects into the calculation of the contact density [7,17–19]. The two requirements can be the most elegantly achieved with the use of the analytic derivative formalism [5,20] where the contact density is represented in terms of the derivative of the electronic energy with respect to the nuclear charge radius. The initial application of this formalism to compounds of Fe, Sn, and Hg [7,15–17,20,21] proved its accuracy and efficiency; which were improved by the development of fully analytic computation of the derivatives [19].

In 1997 Dyll [22] derived the normalised elimination of the small component (NESC) Hamiltonian, which triggered development of eXact 2-Component (X2C) [23–27] and Infinite Order Two-Component (IOTC) Hamiltonians [28] in the following decades. Compared to the previous approximate quasi-relativistic Hamiltonians, e.g. ZORA [29], IORA [30], or DKH [31,32], the X2C and IOTC Hamiltonians are exact for one-electron systems, e.g. H-like atomic ions [33], and are free of picture change errors (PCE) except the two-electron (2e)

PCE [27]; this prompted the use of the ‘Dirac-exact’ prefix in connection with these methods [33,34] instead of a zoo of peculiar acronyms, see e.g. in Ref. [35]. The Dirac-exact NESC formalism (denoted later on as NESC, for simplicity) is distinguished from a variety of alternative Hamiltonians by its conceptual simplicity, which enabled derivation and implementation of the analytic derivatives formalism for the calculation of analytic gradients [36,37], vibrational frequencies and IR intensities [38,39], and other atomic and molecular properties [40], such as the contact densities and hyperfine structure constants [19,41,42], electric field gradients [43], electric dipole moments and polarisabilities [44], nuclear magnetic shielding constants [45], and so on. Some of the properties, e.g. the electric response properties and the nuclear magnetic shieldings are available at both the spin-free (sf; or one-component, 1c) NESC level and the two-component (2c) NESC level [46] (Note that there is a typo in the screening factors of mSNSO: $Q(p) = 2.34 \text{Erf}(34500/\alpha_p)$ should be $Q(p) = 2.34 \text{Erf}[(34500/\alpha_p)^2]$); others only at the 1c-NESC level. In addition, the analytic derivatives of X2C (in either the 1c or 2c formalism) have also been developed in other groups [47–50], mainly by Cheng and Gauss. Although the NESC Hamiltonian is equivalent to X2C (e.g. the one-step solution of the NESC equations was already presented by Dyll in Ref. [22]), which implies that within the one-electron approximation 1c-NESC = sf-X2C = X1C and 2c-NESC = X2C, we prefer to stick to using the name NESC in a series of our publications for continuity and to underline the contribution of Ken Dyll to the field of relativistic quantum chemistry [34].

In the present work, the previously available spin-free approach to the calculation of the contact densities and Mössbauer isomer shifts [19] will be extended to the 2c-NESC Hamiltonian. The paper is organised as follows. In Section 2, the methodology of calculating the contact density with the use of the analytic derivatives formalism for 2c-NESC will be described. Details of the calculations performed with the new methodology will be described in Section 3, and the results of the application using the new theory to a series of compounds containing iodine, gold, and mercury atoms will be presented in Section 4. In Section 5, the conclusions will be drawn.

2. Theory

2.1. Contact density and Mössbauer isomer shift

Within the analytic derivative formalism [19,20] the contact density $\bar{\rho}_A$ of nucleus A with the atomic number Z_A is defined as the derivative of the total electronic energy

with respect to the nuclear charge radius, i.e.

$$\bar{\rho}_A = \frac{1}{2\pi} \frac{1}{Z_A \zeta_A^0} \left. \frac{\partial E(\zeta_A)}{\partial \zeta_A} \right|_{\zeta_A = \zeta_A^0}, \quad (2)$$

where ζ_A is the parameter related to the root-mean-square (RMS) charge radius of the nucleus A as

$$\zeta_A = \sqrt{\frac{2}{3}} \langle R_A^2 \rangle^{1/2} \quad (3)$$

and ζ_A^0 is obtained from the experimentally measured or theoretically estimated RMS charge radius of the nucleus A [51–54]. The parameter ζ_A originates from approximating the nuclear charge distribution by a Gaussian-type function; for a point-charge nucleus, $\zeta_A^0 = 0$. With the use of the Gaussian-type nuclear charge distribution, the operator for the electron-nuclear attraction energy V becomes

$$V(\mathbf{r} - \mathbf{R}_A, \zeta_A) = -\frac{Z_A}{|\mathbf{r} - \mathbf{R}_A|} \operatorname{erf}\left(\frac{|\mathbf{r} - \mathbf{R}_A|}{\zeta_A}\right). \quad (4)$$

Therefore, the energy derivative with respect to ζ_A in Equation (2) is given by

$$\left. \frac{\partial E(\zeta_A)}{\partial \zeta_A} \right|_{\zeta_A = \zeta_A^0} = \operatorname{tr} \mathbf{P} \left(\frac{\partial \mathbf{H}_{1e}}{\partial \zeta_A} \right)_{\zeta_A = \zeta_A^0}, \quad (5)$$

where \mathbf{P} is the density matrix and \mathbf{H}_{1e} is the one-electron core Hamiltonian matrix.

From the contact densities at the absorbing and the reference nuclei ($\bar{\rho}_A$ and $\bar{\rho}_R$), respectively, the Mössbauer isomer shift can be obtained using Equation (1).

2.2. 2c-NESC and its analytic derivatives formalism

Within the commonly used one-electron approximation to the NESC method [22], the relativistic one-electron Hamiltonian $\tilde{\mathbf{L}}$ renormalised on the non-relativistic metric

$$\mathbf{H}_{1e}^{\text{NESC}} = \mathbf{G}^\dagger \tilde{\mathbf{L}} \mathbf{G} \quad (6)$$

is used in connection with the non-relativistic electron-electron repulsion terms. The NESC Hamiltonian matrix $\tilde{\mathbf{L}}$ [22] and the renormalisation matrix \mathbf{G} [55] are given by

$$\tilde{\mathbf{L}} = \mathbf{T}\mathbf{U} + \mathbf{U}^\dagger \mathbf{T} - \mathbf{U}^\dagger (\mathbf{T} - \mathbf{W})\mathbf{U} + \mathbf{V}, \quad (7)$$

$$\mathbf{G} = \mathbf{S}^{-1/2} \left[\mathbf{S}^{1/2} \left(\mathbf{S} + \frac{1}{2c^2} \mathbf{U}^\dagger \mathbf{T} \mathbf{U} \right)^{-1} \mathbf{S}^{1/2} \right]^{1/2} \mathbf{S}^{1/2}, \quad (8)$$

where \mathbf{S} is the overlap matrix, \mathbf{T} is the kinetic energy matrix, \mathbf{V} is the potential energy matrix, \mathbf{W} is the matrix of the operator $(\boldsymbol{\sigma} \cdot \mathbf{p})V(\mathbf{r})(\boldsymbol{\sigma} \cdot \mathbf{p})/(4c^2)$ (where \mathbf{p} is the momentum operator, $\boldsymbol{\sigma}$ is the vector of the three Pauli

spin matrices, and c is the velocity of light), and \mathbf{U} is the matrix which connects the large component \mathbf{C}_+^L and the small component \mathbf{C}_+^S of the positive-energy, i.e. electronic solutions of the Dirac matrix equation, $\mathbf{C}_+^S = \mathbf{U}\mathbf{C}_+^L$ [22].

In the case of 2c-NESC, all the matrices in the above equations are in the 2c form, i.e. $\mathbf{X}_{2c} = \mathbf{I}_2 \cdot \mathbf{X}_{1c}$ (\mathbf{I}_2 is a 2×2 unit matrix; $\mathbf{X} = \mathbf{S}, \mathbf{T}$, or \mathbf{V}), $\mathbf{W} = \mathbf{I}_2 \cdot \mathbf{W}^{sf} + i\boldsymbol{\sigma} \cdot \mathbf{W}^{so}$, and the other matrices can be obtained using these four matrices. The spin-orbit coupling is incorporated into the 2c-NESC method using a modified version of the screened-nuclear-spin-orbit (SNSO) approach [46], proposed originally by Boettger [56], i.e. the 2e-SOC contributions are not calculated explicitly but simulated by the nuclear screening factors in the one-electron SOC integrals. With the SNSO approximation, the \mathbf{W} matrix in Equation (7) is replaced by [37]

$$\begin{aligned} \mathbf{W}^{\text{SNSO}} &= \mathbf{I}_2 \cdot \mathbf{W}^{sf} + i\boldsymbol{\sigma} \cdot (\mathbf{W}_{so} - \mathbf{Q}\mathbf{W}_{so}\mathbf{Q}) \\ &= \mathbf{W} - \mathbf{Q}(\mathbf{W} - \mathbf{I}_2 \cdot \mathbf{W}^{sf})\mathbf{Q}, \end{aligned} \quad (9)$$

where \mathbf{Q} is a diagonal matrix containing the square roots of the SNSO factors as its diagonal elements.

A derivative of the NESC Hamiltonian (both 1c and 2c) with respect to a general external perturbation λ is given by [37]

$$\begin{aligned} \operatorname{tr} \mathbf{P} \frac{\partial \mathbf{H}_{1e}^{\text{NESC}}}{\partial \lambda} &= \operatorname{tr} \mathbf{P}_S \frac{\partial \mathbf{S}}{\partial \lambda} + \operatorname{tr} \mathbf{P}_T \frac{\partial \mathbf{T}}{\partial \lambda} \\ &\quad + \operatorname{tr} \mathbf{P}_V \frac{\partial \mathbf{V}}{\partial \lambda} + \operatorname{tr} \mathbf{P}_W \frac{\partial \mathbf{W}}{\partial \lambda}, \end{aligned} \quad (10)$$

where \mathbf{P}_S , \mathbf{P}_T , \mathbf{P}_V , and \mathbf{P}_W are given in Equations (22)–(23) of Ref. [37]. Within the SNSO approximation, the last term in Equation (10) becomes [37]

$$\begin{aligned} \operatorname{tr} \mathbf{P}_W \frac{\partial \mathbf{W}^{\text{SNSO}}}{\partial \lambda} &= \operatorname{tr} (\mathbf{P}_W - \mathbf{Q}\mathbf{P}_W\mathbf{Q}) \frac{\partial \mathbf{W}}{\partial \lambda} \\ &\quad + \operatorname{tr} \mathbf{Q}\mathbf{P}_W\mathbf{Q} \left(\mathbf{I}_2 \cdot \frac{\partial \mathbf{W}^{sf}}{\partial \lambda} \right). \end{aligned} \quad (11)$$

Although the previous study [19] found that, for the first-order electronic properties, the contributions of the $\partial \mathbf{U}/\partial \lambda$ derivatives are insignificant, these contributions are retained in the present formalism, as their calculation requires only a few matrix multiplications and leads to an insignificant computational overhead (*c.f.* Ref. [37] and references therein). These contributions are folded into the \mathbf{P}_X matrices ($X = S, T, V$, and W) in Equation (10) [37].

It is noteworthy that besides SNSO there are also other ways to include 2e-SO contributions, see e.g. Refs. [57–59]. If the approximate 2e-SO contributions do not

depend on the perturbation parameter λ , the general derivative formula in Equation (10) still works in this case.

In the case of the contact density calculation, the general derivative in Equation (10) simplifies due to the independence of the kinetic energy and the overlap matrices on the nuclear charge radius ζ_A , and Equation (2) becomes

$$\bar{\rho}_A = \frac{1}{2\pi} \frac{1}{Z_A \zeta_A^0} \text{tr} \left[\mathbf{P}_V \left(\frac{\partial \mathbf{V}}{\partial \zeta_A} \right)_{\zeta_A = \zeta_A^0} + \mathbf{P}_W \left(\frac{\partial \mathbf{W}}{\partial \zeta_A} \right)_{\zeta_A = \zeta_A^0} \right]. \quad (12)$$

The analytic derivatives of \mathbf{V} and \mathbf{W} (including \mathbf{W}^{sf} and \mathbf{W}^{so}) are calculated by the quadrature developed by Taketa *et al.* [60]. As the 2e-SOC contributions simulated in this work by SNSO, see Equation (11), do not depend on the nuclear charge radius, the derivatives $\partial \mathbf{W} / \partial \zeta_A$ should be taken without including these factors, i.e. without the \mathbf{Q} matrices in Equation (11). This is different from the general derivatives, such as the analytic gradient, where the simulated 2e-SOC contributions were dependent on the perturbation.

3. Computational details

The formalism described in Section 2 was implemented in the COLOGNE2016 suite of programmes [61]. Three sets of calculations were carried out at the HF, PBE0 [62,63], and CAM-B3LYP [64] levels of theory, respectively, in connection with the non-relativistic (NR), 1c-NESC, and 2c-NESC Hamiltonians. The density functionals PBE0 and CAM-B3LYP had been successfully used for the test suite of molecules in our previous papers [36–39,44], so they were adopted in the present work without any further testing. The nuclear charge radii from the compilation by Visscher and Dyllal [53] were used for the nuclear charge distributions. The molecular geometries were taken from Refs. [19,44]. Uncontracted all-electron basis sets were used in this work, where the exponents of primitive Gaussian functions were taken from Refs. [65–70]

- (1) Dyllal's CVQZ basis set [69] for iodine atom in I^- , IX ($X = \text{H, F, Cl, and Br}$), and I_2 . The original basis set was augmented by one tight s-function and one tight p-function ($\alpha_s = 221179043.7$ and $\alpha_p = 188559790.9$).
- (2) Dyllal's CVQZ basis set [68,70] for gold atom in Au^+ and AuX ($X = \text{H, F, Cl, Br, and I}$). The original basis set was augmented by two tight s-functions and one tight p-function ($\alpha_s = 560256407.3, 165482710.2$, and $\alpha_p = 232179879.3$).
- (3) The **B5** basis set [44] for $X = \text{H, F, Cl, Br, and I}$ in IX and AuX .

- (4) Modified Dyllal's CVQZ basis set [68,70] proposed by Knecht *et al.* [7] for the Hg atom in Hg, HgX_n ($n = 2$ and 4; $X = \text{H, F, Cl, Br, and I}$), $\text{Hg}(\text{SH})_4$, $\text{Hg}(\text{CH}_3)_2$, and $\text{Hg}(\text{H}_2\text{O})_6^{2+}$, and **B10** [44] for the other atoms in these molecules.

Due to the absolute contact density values by DFT strongly depend on the grids distributed in the core region, ultrafine grids were always used [7,71].

4. Results and discussion

The results of the calculations are collected in three tables: Table 1 presents the result for IX ($X = \text{H, F, Cl, Br, and I}$) molecules, Table 2 for AuX molecules, and Table 3 for mercury compounds (HgX_2 , HgX_4 , $\text{Hg}(\text{SH})_4$, $\text{Hg}(\text{CH}_3)_2$, and $\text{Hg}(\text{H}_2\text{O})_6^{2+}$). The absolute contact densities are given for bare I^- , Au^+ , and Hg atoms and the contact densities for molecules are given by the differences $\Delta \bar{\rho}_M = \bar{\rho}_M^{(mol)} - \bar{\rho}_M^{(atom)}$ ($M = \text{I, Au, or Hg}$).

The quality of a theoretical calculation can be judged by three criteria, i.e. (1) the size of the basis set, (2) the level of treatment of the electron correlation, and (3) the level of inclusion of the relativistic effects [72,73]. The modified CVQZ basis functions used in this work are sufficiently complete and their further extension does not significantly result in changing the contact densities obtained by the analytic derivatives formalism [19]. Hence, the quality of the contact densities obtained in this work depends on the two remaining criteria, i.e. the quantum chemical methodology (HF, PBE0, and CAM-B3LYP) and the relativistic effects (NR, 1c-NESC, and 2c-NESC Hamiltonians).

Table 1. Contact densities (in bohr⁻³) in the first set of NR, 1c-NESC, and 2c-NESC calculations. The absolute contact densities are given for the atom whereas for the molecules the contact density differences are listed.

Method	Molecule	NR	1c-NESC	2c-NESC	Δ_{SF}	Δ_{SO}
HF	I^-	103735.64	237998.24	238372.17		
	IF	2.61	6.95	7.33	4.34	0.38
	ICl	2.31	6.09	6.47	3.78	0.39
	IBr	2.19	5.74	6.05	3.55	0.31
	I_2	1.91	5.03	5.05	3.12	0.01
PBE0	IH	0.73	2.02	2.01	1.30	-0.01
	I^-	103766.03	238684.89	239059.39		
	IF	2.40	6.10	6.35	3.70	0.26
	ICl	2.13	5.34	5.63	3.21	0.30
	IBr	2.03	5.04	5.27	3.01	0.23
CAM-B3LYP	I^-	103776.18	239038.74	239417.31		
	IF	2.63	6.69	6.95	4.07	0.26
	ICl	2.31	5.84	6.12	3.52	0.29
	IBr	2.20	5.49	5.71	3.30	0.22
	I_2	1.94	4.87	4.87	2.93	0.00
	IH	0.69	1.86	1.85	1.17	-0.01

Comparing the total atomic contact densities, it can be seen that $\bar{\rho}_M^{(atom)}$ is very sensitive to the inclusion of the scalar-relativistic effects; the contact density of I^- , see Table 1 increases by a factor of two, and the contact densities of Au^+ (Table 2) and Hg (Table 3) increase by almost an order of magnitude. However, the inclusion of SOC through the 2c-NESC formalism leads to a minor increase of $\bar{\rho}_M^{(atom)}$, by *ca.* 0.2–1%. The enhancement of the contact density in the scalar-relativistic calculations is caused by contraction of the atomic *ns*-orbitals, as only these orbitals have non-vanishing density at the nucleus. In 2c-NESC, the $np_{1/2}$ -spinors acquire also non-zero magnitude at the nuclear position due to SOC. The latter effect however is much less significant than the density enhancement due to the orbital contraction.

The contact density for IX at the iodine nucleus increases in the sequence $H < I < Br < Cl < F$. Iodine has the valence electronic configuration $5s^25p^5$. When the electron density is withdrawn from the *s*-type valence orbital, the contact density decreases due to direct depletion of the density at the nucleus (only *s*-type orbitals have non-zero density at the nucleus) [15,74]. However, when the density is withdrawn from other valence orbitals, e.g. *p*-type or *d*-type orbitals, the contact density increases due to decrease of the screening of the nuclear charge by these electrons [15,74]. Hence, in the IX series, the more electronegative ligands withdraw more *5p*-electrons and this results in an increase of the contact density at the iodine nucleus. That the density is withdrawn from the *p*-type orbitals as illustrated by Figure 1 which shows the difference density between the IF molecule and I^- atom. The difference density has mainly *p*-orbital symmetry.

For the AuX and HgX_2 molecules, the contact density decreases in the sequence $H < I < Br < Cl < F$, which

Table 3. Contact densities (in bohr⁻³) in the third set of NR, 1c-NESC, and 2c-NESC calculations. See the explanations in Table 1.

Method	Molecule	NR	1c-NESC	2c-NESC	Δ_{SF}	Δ_{SO}
HF	Hg	359538.5	2103759.7	2122364.4		
	HgF ₂	-13.0	-115.2	-112.7	-102.1	2.4
	HgCl ₂	-11.6	-106.5	-104.3	-94.9	2.1
	HgBr ₂	-11.9	-107.8	-105.8	-95.9	2.0
	Hgl ₂	-10.5	-96.5	-93.7	-86.0	2.8
	HgH ₂	-3.8	-48.5	-45.4	-44.7	3.1
	HgF ₄	-6.6	-91.9	-87.2	-85.3	4.7
	HgCl ₄	-8.5	-95.1	-90.6	-86.6	4.5
	HgBr ₄	-9.6	-99.9	-96.0	-90.4	4.0
	Hgl ₄	-10.3	-103.2	-99.4	-92.8	3.8
	HgH ₄	-1.2	-44.1	-37.8	-42.9	6.3
	Hg(SH) ₄	-7.4	-84.2	-79.5	-76.8	4.7
	Hg(CH ₃) ₂	-3.5	-46.3	-43.1	-42.9	3.2
	Hg(H ₂ O) ₆ ²⁺	-22.3	-235.0	-235.8	-212.6	-0.8
	PBE0	Hg	359605.8	2112546.8	2131274.5	
HgF ₂		-13.1	-100.7	-98.4	-87.6	2.4
HgCl ₂		-12.2	-94.2	-92.1	-82.0	2.0
HgBr ₂		-12.3	-92.8	-91.0	-80.5	1.8
Hgl ₂		-11.1	-83.4	-80.7	-72.2	2.7
HgH ₂		-4.6	-44.6	-42.1	-40.0	2.6
HgF ₄		-11.5	-107.8	-103.4	-96.3	4.4
HgCl ₄		-11.8	-102.4	-98.4	-90.6	3.9
HgBr ₄		-12.2	-101.7	-98.3	-89.5	3.4
Hgl ₄		-12.6	-99.7	-95.9	-87.0	3.7
HgH ₄		-4.1	-53.8	-48.4	-49.7	5.4
Hg(SH) ₄		-10.5	-91.1	-87.1	-80.6	4.0
Hg(CH ₃) ₂		-4.9	-46.8	-44.2	-42.0	2.6
Hg(H ₂ O) ₆ ²⁺		-23.9	-220.9	-220.6	-197.0	0.3
CAM-B3LYP		Hg	359629.7	2113901.8	2132649.4	
	HgF ₂	-13.5	-103.4	-101.0	-89.9	2.5
	HgCl ₂	-12.6	-96.3	-94.2	-83.7	2.1
	HgBr ₂	-12.7	-95.0	-93.0	-82.2	2.0
	Hgl ₂	-11.5	-85.1	-82.2	-73.6	2.9
	HgH ₂	-5.1	-47.7	-45.0	-42.6	2.7
	HgF ₄	-11.7	-108.8	-104.3	-97.1	4.5
	HgCl ₄	-12.0	-102.8	-98.7	-90.8	4.1
	HgBr ₄	-12.4	-102.2	-98.6	-89.8	3.6
	Hgl ₄	-12.8	-100.2	-96.2	-87.4	4.0
	HgH ₄	-4.7	-57.1	-51.5	-52.4	5.6
	Hg(SH) ₄	-10.6	-91.5	-87.3	-80.9	4.2
	Hg(CH ₃) ₂	-5.3	-48.8	-46.1	-43.6	2.8
	Hg(H ₂ O) ₆ ²⁺	-24.2	-222.5	-222.1	-198.2	0.4

Table 2. Contact densities (in bohr⁻³) in the second set of NR, 1c-NESC, and 2c-NESC calculations. See the explanations in Table 1.

Method	Molecule	NR	1c-NESC	2c-NESC	Δ_{SF}	Δ_{SO}	
HF	Au ⁺	346185.0	1946896.5	1963140.0			
	AuF	5.8	84.1	88.8	78.3	4.7	
	AuCl	7.6	98.0	100.9	90.4	2.9	
	AuBr	7.7	98.9	101.1	91.2	2.2	
	AuI	8.4	105.0	107.0	96.6	2.0	
	AuH	15.2	166.4	167.7	151.2	1.3	
	PBE0	Au ⁺	346247.0	1955189.4	1971539.7		
		AuF	8.5	112.5	118.9	104.0	6.3
AuCl		10.3	124.7	128.3	114.5	3.6	
AuBr		10.5	126.8	129.2	116.2	2.4	
AuI		11.3	133.1	135.4	121.8	2.3	
AuH		18.6	187.1	189.1	168.5	1.9	
CAM-B3LYP		Au ⁺	346270.3	1957434.7	1973806.6		
		AuF	8.1	107.1	112.9	99.0	5.8
	AuCl	9.8	120.3	123.5	110.5	3.2	
	AuBr	10.1	122.7	124.8	112.6	2.1	
	AuI	10.9	129.7	131.7	118.8	2.0	
	AuH	18.1	182.9	184.6	164.8	1.7	

suggests that the direct mechanism of the contact density depletion (due to the density withdrawal from the valence *ns*-orbitals) is involved. Indeed, both Au and Hg atoms have the valence *6s*-shell occupied with one and two electrons, respectively. Formation of chemical bond with a more electronegative element results in a density withdrawal from the valence *ns*-orbital; e.g. the latter reaches *ca.* 1.37 \bar{e} for HgF₂ by NBO analysis [75,76].

In the HgX_4 series, the variation of the contact density occurs in the opposite directions depending on the inclusion of relativity and electron correlation. The HF calculations, with both non-relativistic and relativistic Hamiltonians, predict that the contact density at Hg decreases in the sequence $I < Br < Cl < F < H$. The same ordering of contact densities is predicted by the NR DFT calculations. However, the relativistic DFT

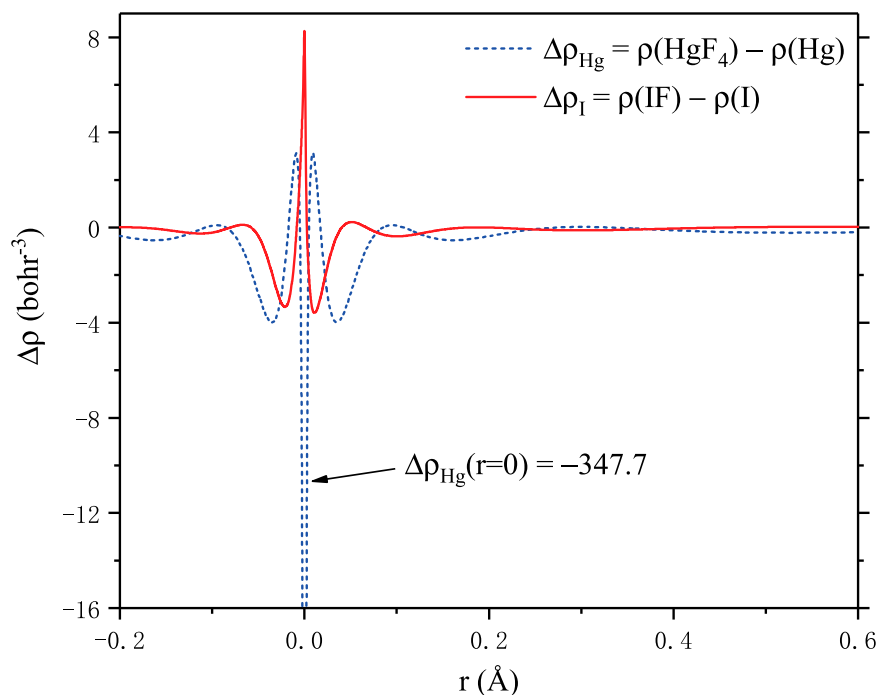


Figure 1. Distributions of electronic density difference by 1c-NESC/HF between molecule and isolated atom along the chemical bonds in HgF_4 and IF . The Hg and I atoms lie at $r = 0 \text{ \AA}$.

calculations overturn the trend to $\text{F} < \text{Cl} < \text{Br} < \text{I} < \text{H}$. The difference between these sets of calculations is likely caused by the interplay between the direct and indirect effects of the ligands on the contact density at the central atom. To clarify this, MP2 and CCSD without frozen cores, i.e. MP2(full) and CCSD(full), combined with the 1c-NESC Hamiltonian have also been performed for HgF_4 and HgCl_4 , where the basis functions of F and Cl are contracted for the sake of computational efficiency. It is found that $\Delta\bar{\rho}_{\text{Hg}}$ is increased by 9.7 (MP2) or 2.6 bohr^{-3} (CCSD) from HgF_4 to HgCl_4 , confirming our relativistic DFT results qualitatively.

Indeed, the Hg atom in HgX_4 molecules behaves as a transition metal atom, i.e. the $5d$ -orbitals of mercury take part in the bonding [77]. For the contact density this means that its variations can be caused by the direct mechanism (withdrawal from the $6s$ -orbital) as well as by the indirect mechanism (withdrawal from the $5d$ -orbitals). The involvement of the $5d$ -orbitals in bonding depends on the Hg–X bondlength; the shorter the latter, the greater the former. Apparently, at the NR and NESC/HF levels, the direct decrease of the contact density due to the withdrawal from the $6s$ -orbital is largely compensated by the indirect increase due to the withdrawal from the $5d$ -orbitals. Hydrogen is the least electronegative atom among the X atoms and withdraws only a small fraction of density from Hg; which leads to a quite small $\Delta\bar{\rho}$ value, see Table 3. Fluorine is the most electronegative atom and withdraws the greatest amount of

density ($Q_{\text{Hg}} = 2.08\bar{e}$ by NBO), however due to a relatively short Hg–F distance (1.882 Å) the involvement of the $5d$ -orbitals in the HgF bonding is substantial [77]. Hence, the direct and the indirect mechanisms largely compensate each other and the contact density at Hg decreases less than for the other halogen ligands. For heavier halogens, the Hg–X distance increases and the involvement of the $5d$ -orbitals of Hg fades away and the contact density at Hg is mostly influenced by the withdrawal from the $6s$ -orbital. Hence, the contact density at Hg decreases more with I than with F.

Judging from Table 3, this explains the trends in the NR and NESC/HF calculations. However, for the NESC/DFT calculations with both density functionals an opposite trend holds, where the most electronegative ligand leads to the greatest decrease of the contact density at Hg. This suggests the dominance of the direct mechanism (withdrawal from the $6s$ -orbital of Hg) for the final contact density $\bar{\rho}_{\text{Hg}}$. Analysis of the natural electron configurations by NBO shows that the electronic density withdrawal from the $5d$ -orbitals slightly decreases from the 1c-NESC/HF to 1c-NESC/PBE0 (the total population $n_{5d}^{\text{HF}} = 9.07\bar{e}$ and $n_{5d}^{\text{PBE0}} = 9.26\bar{e}$), whereas the withdrawal from the $6s$ -orbitals remains almost unchanged ($n_{6s}^{\text{HF}} = 0.51\bar{e}$ and $n_{6s}^{\text{PBE0}} = 0.58\bar{e}$). Hence, the inclusion of relativity together with electron correlation results in changing the balance between the direct and the indirect effects on the Hg contact density. The results of Table 3 clearly show that the relativity and correlation are not additive and

should always be included together in the calculations and not by the respective increments.

Comparing the contact densities obtained at the non-relativistic, scalar-relativistic, and 2c level of theory the significance of various relativistic effects can be evaluated. The values of increments $\Delta_{SF} = \Delta\bar{\rho}^{(1c-NESC)} - \Delta\bar{\rho}^{(NR)}$ and $\Delta_{SO} = \Delta\bar{\rho}^{(2c-NESC)} - \Delta\bar{\rho}^{(1c-NESC)}$ of the contact density due to the scalar-relativistic and SOC effects, respectively, are listed in Tables 1–3. The scalar-relativistic effects result in a two-fold increase of the contact density at iodine $\Delta\bar{\rho}_I$ and more than an order of magnitude increase of $\Delta\bar{\rho}_{Au}$ and $\Delta\bar{\rho}_{Hg}$. By contrast, the effects of SOC contribute generally *ca.* < 5% to the contact density differences, as was also previously observed by Knecht *et al.* [7], however can be as large as 10% for HgH_4 . Similar variations are also observed for $Hg(SH)_4$, $Hg(CH_3)_2$, and $Hg(H_2O)_6^{2+}$. Hence, SOC does not make a significant contribution to the contact density variations and $\Delta_{SO} \ll \Delta_{SF}$ for the elements studied here. However, for heavier elements, e.g. the superheavy atoms and their compounds with multiple quasi-degenerate states and strong state-interactions, the contribution of SOC to the contact density may become more significant. This topic is currently under investigation.

Because the two-component *ab initio* wavefunction calculations beyond HF [78–82] are not currently available in COLOGNE2016, the accurate values of the contact density can be evaluated by the use of an incremental scheme, where the contact densities calculated by the use of an advanced *ab initio* method, e.g. such as CCSD or similar, in connection with the 1c-NESC Hamiltonian are incremented by the SOC contributions obtained by the use of 2c-NESC/DFT method. The evaluation of such a composite scheme is currently under way.

5. Conclusions

A fully analytic approach utilising the analytic derivative formalism for the calculation of the contact density was derived and implemented in connection with the Dirac-exact 2c-NESC method. The new method was tested in the calculation of the contact densities of several I-, Au-, and Hg-containing compounds, and the results were compared with the non-relativistic and the scalar-relativistic 1c-NESC ones to evaluate the impact of the spin-orbit coupling. It was found that SOC makes generally only a minor contribution into the total contact density at the heavy nucleus. This contrasts with the significance of the scalar-relativistic effects which may lead to more than an order of magnitude enhancement of the contact density. As the scalar-relativistic calculations with the 1c-NESC Hamiltonian are available in connection with the high level wavefunction *ab initio* methods, an

incremental scheme where the 1c-NESC/*ab initio* contact density is supplemented by the 2c-NESC/DFT contribution can potentially lead to obtaining very accurate contact densities on the nuclei of heavy and super-heavy elements. Exploration of this possibility is currently in progress.

Acknowledgements

We thank SMU for providing computational resources.

Disclosure statement

No potential conflict of interest was reported by the authors.

Funding

This work was financially supported by the Division of Chemistry (National Science Foundation) Grant CHE 1464906.

ORCID

Wenli Zou  <http://orcid.org/0000-0002-0747-2428>

References

- [1] M. Kaupp, M. Bühl and V.G. Malkin, *Calculation of NMR and EPR Parameters: Theory and Applications* (WILEY-VCH Weinheim, Germany, 2004).
- [2] R.L. Mössbauer, *Z. Phys.* **151**, 124–143 (1958).
- [3] J. Bigeleisen, *J. Am. Chem. Soc.* **118**, 3676–3680 (1996).
- [4] D.A. Shirley, *Rev. Mod. Phys.* **36**, 339–351 (1964).
- [5] M. Filatov, *Coord. Chem. Rev.* **253**, 594–605 (2009).
- [6] P. Gülich, E. Bill and A. Trautwein, *Mössbauer Spectroscopy and Transition Metal Chemistry: Fundamentals and Applications* (Springer, Heidelberg, 2011).
- [7] S. Knecht, S. Fux, R. van Meer, L. Visscher, M. Reiher and T. Saue, *Theor. Chem. Acc.* **129**, 631–650 (2011).
- [8] A. Almoukhalalati, A. Shee and T. Saue, *Phys. Chem. Chem. Phys.* **18**, 15406–15417 (2016).
- [9] B.D. Dunlap and G.M. Kalvius, in *Mössbauer Isomer Shifts*, edited by G. K. Shenoy and F. E. Wagner (North-Holland, Amsterdam, 1978), Chap. 2, pp. 15–48.
- [10] P. Gülich, R. Link and A. Trautwein, *Mössbauer Spectroscopy and Transition Metal Chemistry* (Springer, Heidelberg, 1978).
- [11] J. Tuček and M. Miglierini, editors, *Mössbauer Spectroscopy in Materials Science-2010, AIP Conference Series*, Vol. 1258 (AIP, New York, 2010).
- [12] M.D. Dyar, D.G. Argenti, M.W. Schaefer, C.A. Grant and E. Sklute, *Annu. Rev. Earth Planet. Sci.* **34**, 83–125 (2006).
- [13] E. Münck, in *Physical Methods in Bioinorganic Chemistry: Spectroscopy and Magnetism*, edited by L. Que Jr. (University Science Books, Sausalito, 2000), Chap. 6, pp. 287–320.
- [14] E. Münck and A. Stubna, in *Comprehensive Coordination Chemistry II, Fundamentals: Physical Methods, Theoretical analysis and Case Studies*, edited by J. A. McCleverty, T. B. Meyer and A. B. P. Lever, Vol. 2 (Elsevier, New York, 2003), pp. 279–286.
- [15] R. Kurian and M. Filatov, *Phys. Chem. Chem. Phys.* **12**, 2758–2762 (2010).

- [16] R. Kurian and M. Filatov, *J. Phys.: Conf. Ser.* **217**, 012012 (2010).
- [17] R. Kurian and M. Filatov, *J. Chem. Phys.* **130**, 124121 (2009).
- [18] M. Filatov, W. Zou and D. Cremer, *J. Chem. Phys.* **137**, 131102 (2012).
- [19] M. Filatov, W. Zou and D. Cremer, *J. Chem. Theor. Comput.* **8**, 875–882 (2012).
- [20] M. Filatov, *J. Chem. Phys.* **127**, 084101 (2007).
- [21] R. Kurian and M. Filatov, *J. Chem. Theory Comput.* **4**, 278–285 (2008).
- [22] K.G. Dyall, *J. Chem. Phys.* **106**, 9618–9626 (1997).
- [23] W. Kutzelnigg and W. Liu, *J. Chem. Phys.* **123**, 241102 (2005).
- [24] W. Liu and D. Peng, *J. Chem. Phys.* **125**, 044102 (2006).
- [25] W. Liu and D. Peng, *J. Chem. Phys.* **125**, 149901 (2006).
- [26] M. Iliáš and T. Saue, *J. Chem. Phys.* **126**, 064102 (2007).
- [27] W. Liu, *Phys. Rep.* **537**, 59–89 (2014).
- [28] M. Barysz, L. Mentel and J. Leszczynski, *J. Chem. Phys.* **130**, 164114 (2009).
- [29] E. van Lenthe, E.J. Baerends and J.G. Snijders, *J. Chem. Phys.* **99**, 4597–4610 (1993).
- [30] K.G. Dyall and E. van Lenthe, *J. Chem. Phys.* **111**, 1366–1372 (1999).
- [31] M. Douglas and N.M. Kroll, *Ann. Phys. (NY)* **82**, 89–155 (1974).
- [32] B.A. Hess, *Phys. Rev. A* **32**, 756–763 (1985).
- [33] W. Zou, M. Filatov and D. Cremer, *Theor. Chem. Acc.* **130**, 633–644 (2011).
- [34] D. Cremer, W. Zou and M. Filatov, *WIREs Comput. Mol. Sci.* **4**, 436–467 (2014).
- [35] D. Peng and M. Reiher, *Theor. Chem. Acc.* **131**, 1081 (2012).
- [36] W. Zou, M. Filatov and D. Cremer, *J. Chem. Phys.* **134**, 244117 (2011).
- [37] W. Zou, M. Filatov and D. Cremer, *J. Chem. Phys.* **142**, 214106 (2015).
- [38] W. Zou, M. Filatov and D. Cremer, *J. Chem. Theory Comput.* **8**, 2617–2629 (2012).
- [39] W. Zou, M. Filatov and D. Cremer, *J. Chem. Phys.* **137**, 084108 (2012).
- [40] M. Filatov, W. Zou and D. Cremer, *Int. J. Quantum Chem.* **114**, 993–1005 (2014).
- [41] M. Filatov, W. Zou and D. Cremer, *J. Phys. Chem. A* **116**, 3481–3486 (2012).
- [42] M. Filatov, W. Zou and D. Cremer, *Curr. Inorg. Chem.* **3**, 284–290 (2013).
- [43] M. Filatov, W. Zou and D. Cremer, *J. Chem. Phys.* **137**, 054113 (2012).
- [44] T. Yoshizawa, W. Zou and D. Cremer, *J. Chem. Phys.* **145**, 184104 (2016).
- [45] T. Yoshizawa, W. Zou and D. Cremer, *J. Chem. Phys.* **146**, 134109 (2017).
- [46] M. Filatov, W. Zou and D. Cremer, *J. Chem. Phys.* **139**, 014106 (2013).
- [47] L. Cheng and J. Gauss, *J. Chem. Phys.* **135**, 084114 (2011).
- [48] L. Cheng and J. Gauss, *J. Chem. Phys.* **135**, 244104 (2011).
- [49] L. Cheng, J. Gauss and J.F. Stanton, *J. Chem. Phys.* **139**, 054105 (2013).
- [50] Y.J. Franzke, N. Middendorff and F. Weigend, *J. Chem. Phys.* **148**, 104110 (2018).
- [51] E.G. Nadjakov, K.P. Marinova and Y. Gangrsky, *At. Data Nucl. Data Tables* **56**, 133–157 (1994).
- [52] G. Fricke, C. Bernhardt, K. Heilig, L.A. Schaller, L. Schellenberg, E.B. Shera and C.W. de Jager, *At. Data Nucl. Data Tables* **60**, 177–285 (1995).
- [53] L. Visscher and K.G. Dyall, *At. Data Nucl. Data Tables* **67**, 207–224 (1997).
- [54] D. Andrae, *Phys. Rep.* **336**, 413–525 (2000).
- [55] W. Liu and D. Peng, *J. Chem. Phys.* **131**, 031104 (2009).
- [56] J.C. Boettger, *Phys. Rev. B* **62**, 7809–7815 (2000).
- [57] B.A. Hess, C.M. Marian, U. Wahlgren and O. Gropen, *Chem. Phys. Lett.* **251**, 365–371 (1996).
- [58] B. Schimmelpfennig, *AMFI: Atomic Mean Field Integral Program* (University of Stockholm, Stockholm, 1996).
- [59] J. Liu and L. Cheng, *J. Chem. Phys.* **148**, 144108 (2018).
- [60] H. Taketa, S. Huzinaga and K. O-ohata, *J. Phys. Soc. Japan* **21**, 2313–2324 (1966).
- [61] E. Kraka, W. Zou, M. Filatov, T. Yoshizawa, J. Gräfenstein, D. Izotov, J. Gauss, Y. He, A. Wu, V. Polo, L. Olsson, Z. Konkoli, Z. He and D. Cremer, *COLOGNE2016*, Southern Methodist University, Dallas, TX 2016.
- [62] J.P. Perdew, K. Burke and M. Ernzerhof, *Phys. Rev. Lett.* **77**, 3865–3868 (1996).
- [63] C. Adamo and V. Barone, *J. Chem. Phys.* **110**, 6158–6170 (1998).
- [64] T. Yanai, D.P. Tew and N.C. Handy, *Chem. Phys. Lett.* **393**, 51–57 (2004).
- [65] F. Weigend and R. Ahlrichs, *Phys. Chem. Chem. Phys.* **7**, 3297–3305 (2005).
- [66] T. Noro, M. Sekiya and T. Koga, *Theor. Chem. Acc.* **109**, 85–90 (2003).
- [67] T. Noro, M. Sekiya and T. Koga, *Theor. Chem. Acc.* **131**, 1124 (2012).
- [68] K.G. Dyall, *Theor. Chem. Acc.* **112**, 403–409 (2004).
- [69] K.G. Dyall, *Theor. Chem. Acc.* **115**, 441–447 (2006).
- [70] K.G. Dyall and A.S.P. Gomes, *Theor. Chem. Acc.* **125**, 97–100 (2010).
- [71] F. Neese, *Inorg. Chim. Acta* **337**, 181–192 (2002).
- [72] G. Tarczay, A.G. Császár, W. Klopper and H.M. Quiney, *Mol. Phys.* **99**, 1769–1794 (2001).
- [73] A. Kerridge, in *Computational Methods in Lanthanide and Actinide Chemistry*, edited by M. Dolg (John Wiley & Sons, Ltd, Chichester, UK, 2015), p. 122.
- [74] P.R. Brady, J.F. Duncan and K.F. Mok, *Proc. Roy. Soc. Lond. A* **287** (1410), 343–362 (1965).
- [75] E.D. Glendening, J.K. Badenhop, A.E. Reed, J.E. Carpenter, J.A. Bohmann, C.M. Morales, C.R. Landis and F. Weinhold, *NBO 6.0*, Theoretical Chemistry Institute, University of Wisconsin: Madison 2013.
- [76] E.D. Glendening, C.R. Landis and F. Weinhold, *J. Comput. Chem.* **34**, 1429–1437 (2013).
- [77] X. Wang, L. Andrews, S. Riedel and M. Kaupp, *Angew. Chem. Int. Ed.* **46**, 8371–8375 (2007).
- [78] L. Visscher, T.J. Lee and K.G. Dyall, *J. Chem. Phys.* **105**, 8769–8776 (1996).
- [79] S. Yabushita, Z. Zhang and R.M. Pitzer, *J. Phys. Chem. A* **103**, 5791–5800 (1999).
- [80] H.S. Nataraj, M. Kállay and L. Visscher, *J. Chem. Phys.* **133**, 234109 (2010).
- [81] F. Wang, J. Gauss and C. van Wüllen, *J. Chem. Phys.* **129**, 064113 (2008).
- [82] L. Cheng and J. Gauss, *J. Chem. Phys.* **141**, 164107 (2014).